Effects of distance between plates on flows around a cascade of flat plates with acoustic resonance

Hiroshi Yokoyama[1], Katsuya Kitamiya[2], Akiyoshi Iida[4]
Department of Mechanical Engineering, Toyohashi University of Technology, 1-1 Hibarigaoka, Tempaku, Toyohashi-shi, Aichi, 441-8580, Japan

and

Hiroki Yamamoto[3]
SINFONIA TECHNOLOGY CO., LTD., Shiba NBF Tower, 1-30, Shiba-daimon 1-chome, Minato-ku, Tokyo, 105-8564, Japan

To clarify the effects of the distance between the plates on the flow and acoustic fields around a cascade of flat plates, direct simulations of flow and acoustic fields and wind tunnel experiments were performed. The ratio of the distance to the plate thickness was changed from 0.5 to 13.0. For s/b = 3.0, 6.0, the intense resonant acoustic radiation occurs along with the synchronization of the vortex shedding from neighboring plates. The reason why the acoustic radiation becomes weak for the smaller and larger distance are discussed using computational results.

I. Nomenclature

a_0 = freestream sound speed
b = plate thickness
c = streamwise plate length
C_p = pressure coefficient
F_k = inviscid flux vector
F_k = viscid flux vector
f = frequency
M = freestream Mach number
N = number of plates
p = pressure
Q = conserved vector
q = second invariant
Re_b = Reynolds number based on plate thickness b
Re_c = Reynolds number based on plate length c
Re_s = Reynolds number based on distance s
St = Strouhal number
s = distance between plates
T = period

[1] Assistant professor, Toyohashi University of Technology, 1-1 Hibarigaoka, Tempaku, Toyohashi-shi, Aichi, 441-8580, Japan, and non-AIAA Member.
[2] Graduate student, Toyohashi University of Technology, 1-1 Hibarigaoka, Tempaku, Toyohashi-shi, Aichi, 441-8580, Japan, and non-AIAA Member.
[3] Researcher, SINFONIA TECHNOLOGY CO., LTD., Shiba NBF Tower, 1-30, Shiba-daimon 1-chome, Minato-ku, Tokyo, 105-8564, Japan, and non-AIAA Member.
[4] Professor, Toyohashi University of Technology, 1-1 Hibarigaoka, Tempaku, Toyohashi-shi, Aichi, 441-8580, Japan, and non-AIAA Member.

t = time
U_0 = freestream velocity
u, v, w = streamwise, normal and spanwise velocity components
u_h = velocity measured by hot-wire anemometer
x, y, z = streamwise, normal and spanwise coordinates
ρ_0 = freestream density

II. Introduction

Intense acoustic waves are often radiating from flows around a cascade of flat plates as shown in Fig. 1. These configurations exist in many industrial products, such as automotive grilles, heat exchangers, and architectural louvers. In order to establish methods to suppress this noise, the acoustic radiation mechanism must be clarified.

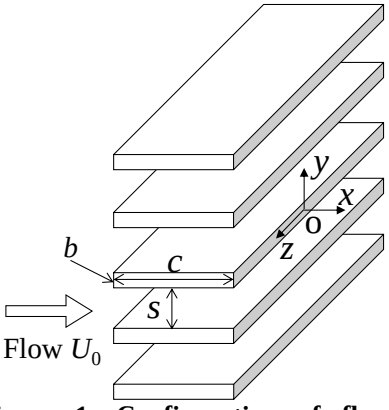

Figure 1. Configuration of flow around a cascade of flat plates.

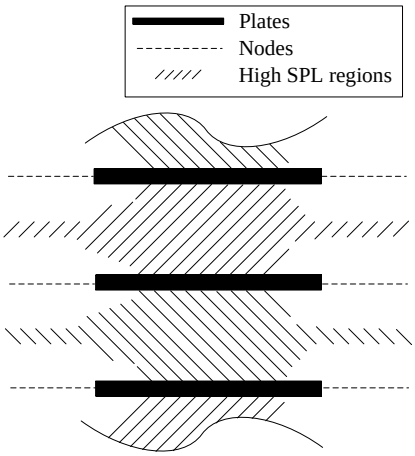

Figure 2. Half-wavelength mode around a cascade of flat plates (mode β proposed by Parker[1]).

Parker[1] measured the sound pressure level for the flows around a cascade of flat plates and clarified that the sound pressure level becomes intense at a specific velocity and that this phenomenon is due to the coupling between the vortex shedding in the wakes and the acoustic resonance between plates as shown in Fig. 2. The effects of acoustic resonance on the flows have been investigated by atuhors[2]. Also, for flows around a cascade of bluff body such as rectangular or circular cylinders, the effects of the distance between the bodies have been found to be significant[3-5]. However, the effects of the distance on the flow and acoustic fields have not been clarified for the cascade of flat plates. In the present study, the effects of the distance between plates on the flow and acoustic fields are focused on.

III. Methodology

A. Flow Configurations

The experimental and computational conditions are showed in Table 1. The plate thickness, b, is 2 mm, and the aspect ratio, C/b, is 15.0. Preliminary experiments have confirmed that acoustic resonance occurs in a half-wavelength mode along the plate length shown in Fig. 2 at U_0 = 44 m/s. In the preliminary experiments, the sound pressure level was measured with the configurations of N = 1-6, C/b = 10-25, and s/b = 2.5-20 ($N \geq 2$) at U_0 = 10-50 m/s, and the resonant frequency of the half-wavelength mode was found to be predicted by the empirical formula

$$f_{\mathrm{res}} = 0.5\left(\frac{a_0}{C}\right)\Bigg/\left(1+\alpha\left(\frac{s}{C}\right)^{\beta}\right), \alpha = 0.7, \beta = 0.84, \quad (1)$$

where a_0 is the sound speed. This half-wavelength mode corresponds to mode β proposed by Parker[1].

Also, preliminary computation for the various ratios of the distance to the plate thickness (s/b = 1.0 - 13.0) at U_0 = 44 m/s presented that the fundamental frequency of the vortex shedding from the plates depends on the ratio, s/b, as follows.

$$St \equiv fb/U_0 = 0.196 + \frac{0.083}{(s/b)}, \tag{2}$$

where the same functional form was used for flows around a cascade of rectangular cylinders[3]. The freestream velocity for the present computations was determined for each distance, s/b, as shown in Table 1 so that the frequency predicted by Eq. (2) agrees with that predicted by Eq. (1) and the above-mentioned coupling between the acoustic resonance and the vortex shedding could occur. At U_0 = 44 m/s, the Reynolds number based on the thickness and the freestream velocity is $\mathrm{Re}_b = 5.8\times10^3$, the Reynolds number based on the length is $\mathrm{Re}_C = 8.7\times10^4$, the Reynolds number based on the distance is $\mathrm{Re}_s = 3.5\times10^4$ for s/b = 6.0 and the freestream Mach number is $M = U_0/a_0$ = 0.13.

Table 1. Computational and experimental parameters.

	Thick. b [m]	Length C/b	Number of plates N	Distance s/b	Velocity U_0 [m/s]	Re_b (U_0 = 44 m/s)	Re_C (U_0 = 44 m/s)
Comp.	2.0×10^{-3}	15.0	5	0.5	30	5.8×10^3	8.7×10^4
				1.0	37		
				1.5	44		
				3.0	46		
				6.0	30, 44, 60		
			1	-	44		
Exp.			5	0.5, 1.0, 1.5, 3.0, 6.0	20-60		
			3	13.0			
			1	-			

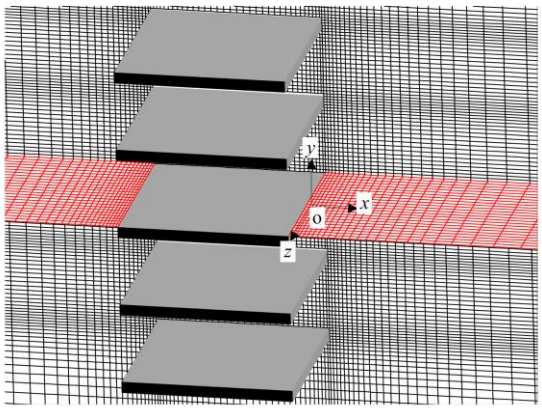

Figure 3. Computational grid near the plates (N = 5, s/b = 6.0). (For clarity, every fifth grid line is shown.)

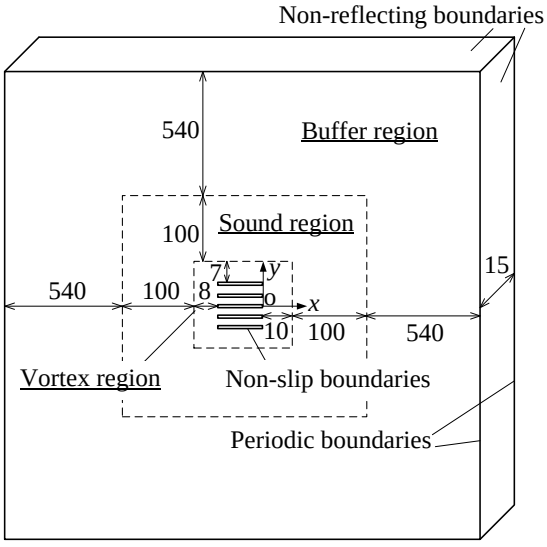

Figure 4. Computational domain and boundary conditions, where the length is non-dimensionalized by the plate thickness, b (N = 5, s/b = 6.0).

B. Computational Methods

1. Governing Equations and Finite Difference Formulation

Flow and acoustic fields were simulated simultaneously by directly solving the three-dimensional compressible Navier-Stokes equations in the conserved form:

$$\boldsymbol{Q}_t + \frac{\partial}{\partial x_k}(\boldsymbol{F}_k - \boldsymbol{F}_{vk}) = 0, \tag{3}$$

where $\boldsymbol{Q}$ is the vector of the conserved variables, $\boldsymbol{F}_k$ is the inviscid flux vector, and $\boldsymbol{F}_{vk}$ is the viscous flux vector. The spatial derivatives were evaluated using the sixth-order-accurate compact finite difference scheme (fourth-order-accurate on the boundaries)[6]. The time integration was performed using the third-order-accurate Runge-Kutta method.

In order to reduce the computational cost, large-eddy simulations (LES) were performed in the present study. The computational grid incorporated into the above-mentioned numerical methods adequately resolves the smallest active vortices in the wakes of the plates. No explicit SGS model was used. The turbulent energy in the GS that should be transferred to SGS eddies is dissipated by a 10th-order spatial filter, as described below. A number of studies have shown[7-9] that the above-mentioned method, which combines low-dissipation discretization schemes and explicit filtering, correctly reproduces turbulent flows. This filter, which is given below, also removes numerical instabilities:[10]

$$\alpha_f \hat{\psi}_{i-1} + \hat{\psi}_i + \alpha_f \hat{\psi}_{i+1} = \sum_{n=0}^{5} \frac{a_n}{2}(\psi_{i+n} + \psi_{i-n}), \tag{4}$$

where ψ is a conserved quantity, and $\hat{\psi}$ is the filtered quantity. The coefficients a_n have the same values as those used by Gaitonde and Visbal[11], and the value of parameter α_f is 0.45.

2. Computational Grids

Figure 3 shows the computational grid for $N = 5$. The spanwise extent of the computational domain is $L_s/b = 15.0$. In the spanwise direction, 120 grid points are used, and the spanwise grid resolution $\Delta z/b = 0.125$ is sufficiently fine to capture the smallest active vortices in the wake as discussed in detail in Ref. 2.

As shown in Fig. 4, the computational domain in the x-y plane is divided into three regions, namely, a vortex region, a sound region, and a buffer region, having different grid spacings.

The spacing in the vortex region is prescribed to be fine enough to analyze the separated shear layer around the upstream edges and the vortical structures in the wake. The spacings adjacent to the plate surface are $\Delta x_{min}/b$ and $\Delta y_{min}/b = 0.05$. In the entire vortex region, $\Delta x/b$ and $\Delta y/b$ are less than 0.2. In the sound region, the spacing is prescribed to be larger than that in the vortex region but still fine enough to capture acoustic waves. The spacings are $\Delta x/b$ and $\Delta y/b \leq 2.0$. In the entire sound region, more than 20 grid points are used per acoustic wavelength of the fundamental frequency, and the acoustic waves are sufficiently captured using the above-mentioned numerical methods. In the buffer region, the grid spacings are stretched to $\Delta x_{max}/b$ and $\Delta y_{max}/b = 50$ in order to dissipate acoustic waves and vortical structures near the artificial boundaries.

3. Boundary Conditions

Figure 1 also summarizes the boundary conditions. The inflow and outflow boundaries are artificial and so must allow vortices and acoustic waves to pass smoothly with minimal numerical disturbances. Non-reflecting boundary conditions based on the characteristic wave relations[12-14] were used at these boundaries. Non-slip and adiabatic boundary conditions were applied at the wall of the plates. The periodic boundary condition was used in the spanwise (z) direction

C. Experimental Methods

The experiments were conducted using the suction-type, low-noise wind tunnel shown in Fig. 5. In the spanwise direction, the test section composed of flat plates was terminated by two end walls, which were constructed of porous plates in order to minimize sound reflections. At a wind speed of 50 m/s, the freestream turbulence intensity was less than 1.0%, the non-uniformity of the mean flow velocity was less than 0.2%. Also, at this velocity, the background noise level was suppressed to less than 73.5 dB (A) with the background noise being measured with the plates removed and all other elements installed..

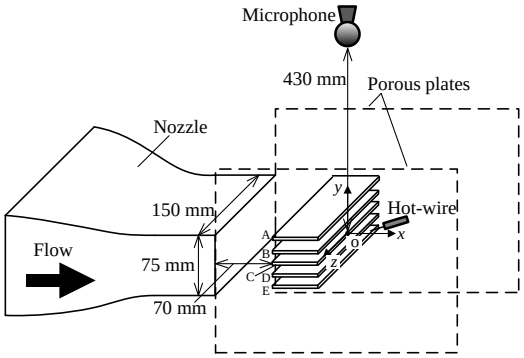

Figure 5. Experimental setup.

IV. Validation of Computational Methods

Figure 6 (a) shows the predicted and measured profiles of the mean values of u_h in the wake (x/b = 2.5) for N = 5 and U_0 = 44 m/s. This position was determined to suppress the effects of the reverse flow in the measurement with the hot-wire anemometer. The predicted mean values are in good agreement with the measured values. Figure 6 (b) shows the predicted and measured RMS values for the fluctuations of u_h. Moreover, the predicted RMS values are in good agreement with the measured values.

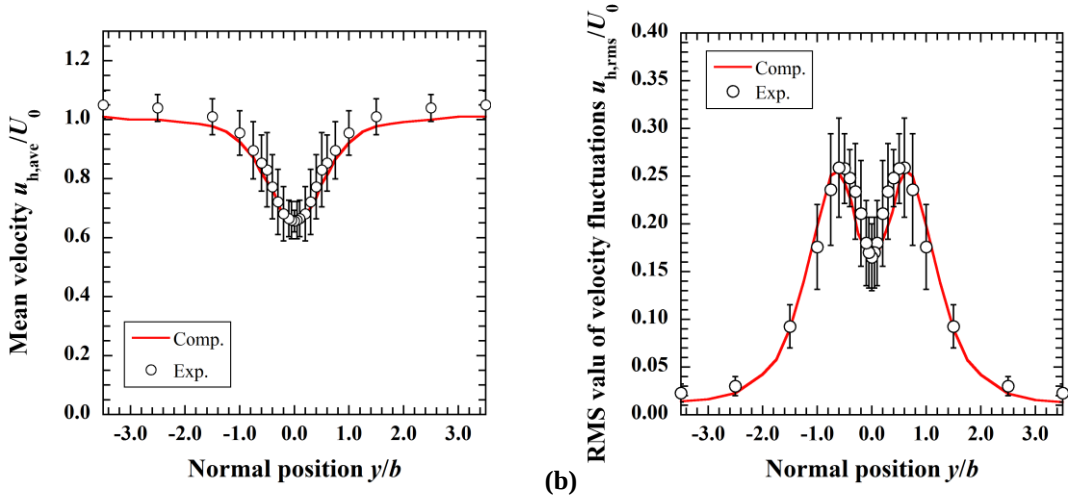

(a) **(b)**

Figure 6. Predicted and measured velocity, u_h, profiles (x/b = 2.5, N = 5, U_0 = 44 m/s). (a) Mean values. (b) RMS values.

Figure 7 shows the predicted and measured levels of the tonal sound in comparison with those for s/b = 3.0 as the function of the ratio of the distance to the plate thickness. In this figure, the level of the tonal sound at the freestream velocity of the condition possible for the resonant acoustic radiation with the agreement of the frequency by Eq. (1) and that by Eq. (2) are plotted for s/b = 0.5-13.0. The level of the tonal sound was estimated by integrating the acoustic power in the frequency range, where the difference in the level from the peak level was within 10 dB. The difference of the freestream velocity was corrected using the sixth power law and the difference of the number of the plates was corrected assumed that the sound power was proportional to the number of the plates. As shown in Fig. 7, both the predicted and measured results show the peak of the level around s/b = 3.0. Figure 8 shows the fundamental frequency as the function of the distance, s/b. The predicted frequencies are also in agreement with those measured.

Along with the discussions of the flow fields in the previous subsection, it was concluded that the present computations adequately capture the flow and acoustic fields.

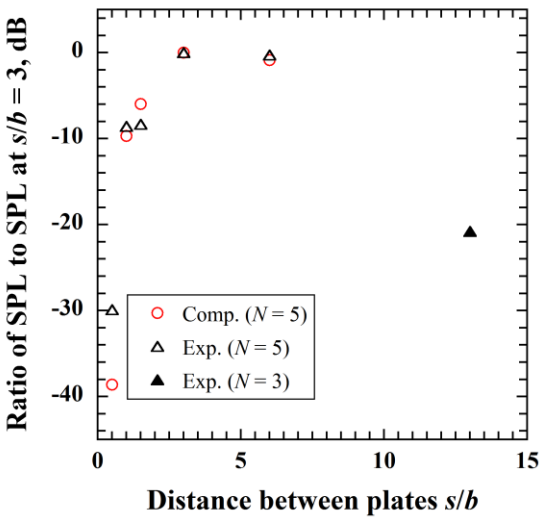

Figure 7. Level of tonal sound as a function of distance between plates *s*/*b*.

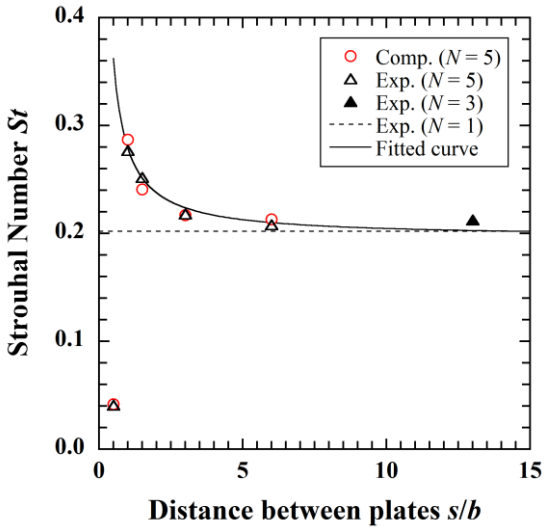

Figure 8. Fundamental Strouhal number as a function of distance between plates *s*/*b*. Fitted curve follows Eq. (2).

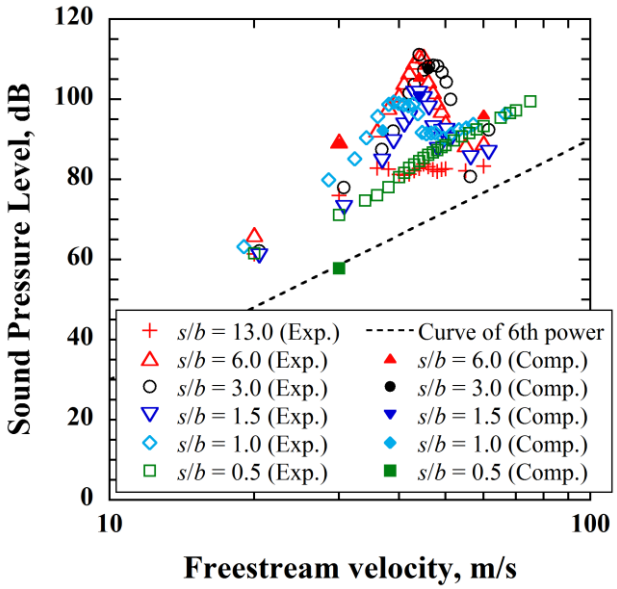

Figure 9. Level of tonal sound as a function of freestream velocity U_0 for N = 5 except measured data at *s*/*b* = 13 (N = 3).

V. Detailed Results

A. Effects of distance on tonal sound

Figure 9 shows the effects of the freestream velocity on the predicted and measured level of the tonal sound for flat plates of N = 3 and 5. The variation of the level has local maximum around 35-50 m/s for *s*/*b* = 1.0-6.0. As shown in Fig. 7, the intense resonant sound is radiating for *s*/*b* = 3.0 and 6.0, whereas the tonal sound is much weaker at *s*/*b* = 0.5 and 13.0. For *s*/*b* = 1.0-6.0, the fundamental frequency for the local maximum was found to

approximately agree with that of the acoustic half-wavelength mode between plates predicted by Eq. (1). These results indicate that the coupling between vortex shedding and acoustic resonance occurs for s/b = 1.0-6.0. Meanwhile, the level approximately follows the 6th power law for s/b = 0.5 and 13.0. For the wide distance of s/b = 13.0, Fig. 8 shows that the fundamental frequency also becomes close to that for a single plate. These results indicates that the flow and acoustic fields around each plate approach those around a single plate for the wide distance of s/b = 13.0. Figure 8 also shows that the fundamental frequency becomes higher as the distance becomes narrower for $s/b \geq 1.0$ and suddenly drops to St = 0.04 at s/b = 0.5. In Sec. V. D, the flow fields for the small distance of s/b = 0.5-1.5 are discussed in detail.

B. Effects of distance on mean velocity field

Figure 10 shows the contours of spanwise-averaged mean velocity u_{ave}. Figure 11 shows the mean velocity profile in the wake of the plates along x/b = 2.5. For s/b = 3.0, 6.0, there is no significant difference among each profile for plates A-E, although the wake is slightly deeper for outer plates (plates A and E). Meanwhile, for the smaller distance of s/b = 0.5-1.5, the biased flow pattern is found. The wakes of plates A, C, E becomes wider and deeper whereas those of plates D, E becomes narrower and shallower. A similar biased flow was observed in flows around side-by-side circular cylinders[5].

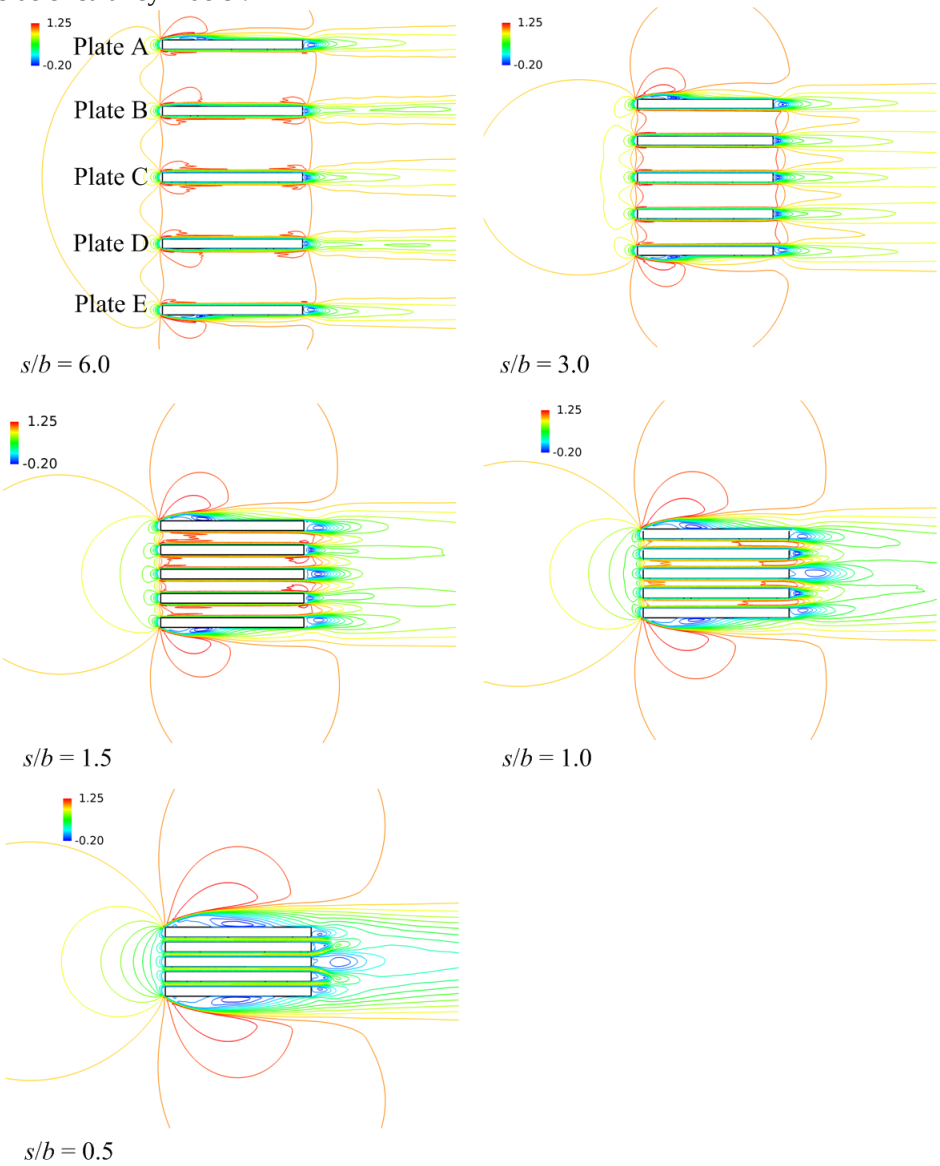

Figure 10. Contours of mean velocity u_{ave}.

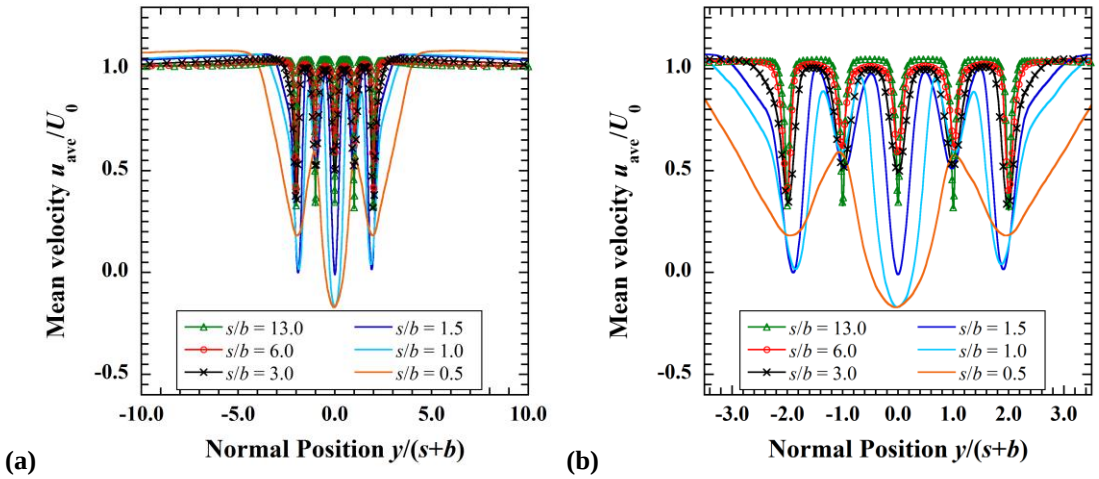

Figure 11. Mean velocity profile along x/b = 2.5. (a) $-20 \le y/b \le 20$. (b) $-3.5 \le y/b \le 3.5$.

C. Coupling between vortex shedding and resonance (s/b = 3.0, 6.0)

Figure 12 shows the effects of the freestream velocity on the level of the tonal sound for N = 1 and 5. For N = 5, the distance between plates is s/b = 6.0. In both the computational and experimental results, there is a peak at U_0 = 44 m/s for N = 5, whereas the level is proportional to the sixth power of the velocity for N = 1. As mentioned above, this indicates that the coupling between the vortex shedding and the acoustic resonance occurs at U_0 = 44 m/s for N = 5.

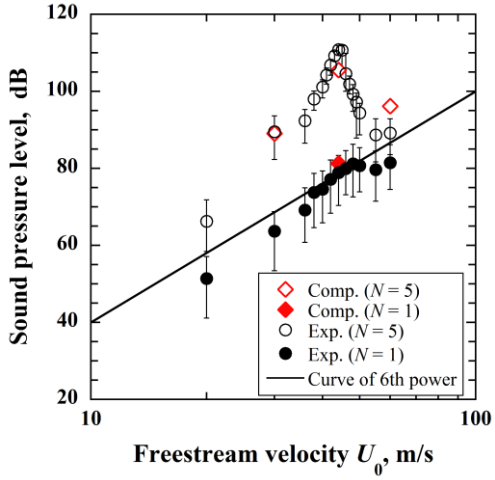

Figure 12. Level of tonal sound as a function of freestream velocity U_0 (s/b = 6.0).

Figure 13 shows the phase- and spanwise-averaged fluctuation pressure fields at this velocity (U_0 = 44 m/s). Phase-averaging was performed by using the velocity fluctuations in the wake at middle plate (plate C in Fig. 3) as reference. As shown in Fig. 13, intense standing waves are formed between the plates and acoustic resonance occurs.

Figure 14 shows fluctuation pressure and iso-surfaces of second invariant for phase-averaged flow fields. Two-dimensional vortices are apparent in the wakes of plate. In both predicted and measured flow fields, the coherence of the velocity fluctuations of the wakes in the spanwise direction and that of the neighboring plates for the resonant conditions were found to be higher than those for off-resonant conditions. This means that the synchronization of vortex shedding from the neighboring plates occurs for the resonant conditions, although this distance of s/b = 6.0 is large enough that synchronization does not occur fluid-dynamically without acoustic resonance[4,5]. This

synchronization is due to the acoustic feedback by the above-mentioned intense standing wave. It has been clarified that the acoustic particle velocity of the standing wave induces the vortical disturbances around the upstream edge[2].

Figure 15 shows the distributions of vorticity for phase- and spanwise-averaged predicted flow fields. Vortex shedding from the neighboring plates was found to be anti-phase mode. Computation of the flow around a single plate was also performed, and the radiation of the acoustic waves from the downstream edge due to vortex shedding from the plate was indicated. When acoustic resonance occurs, vortex shedding in the above-mentioned mode contributes to the intensification of the standing waves between the plates.

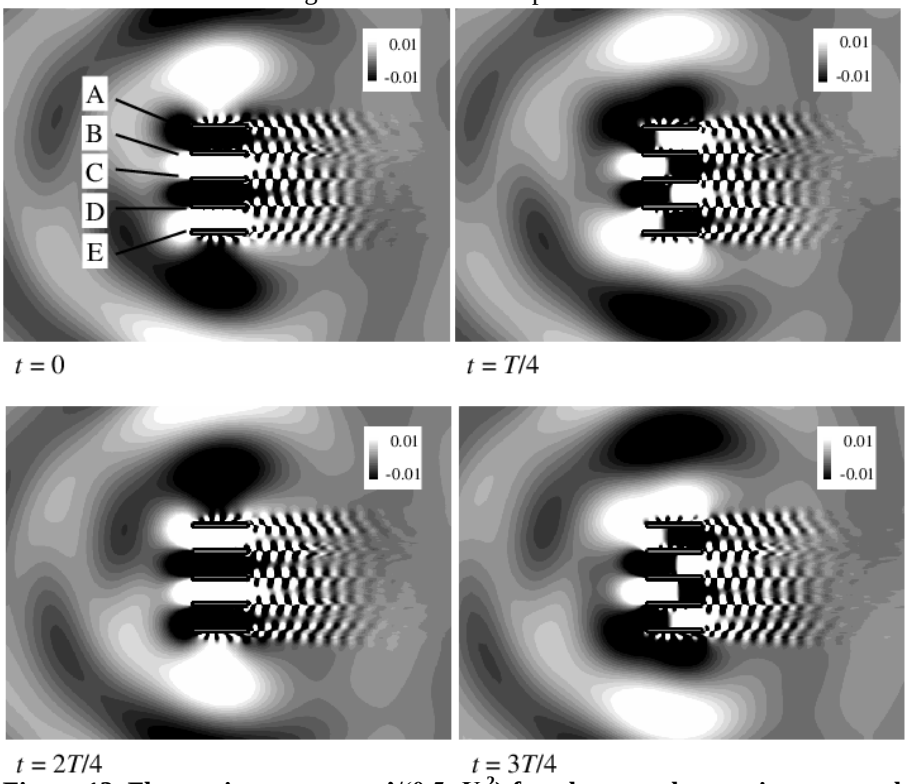

Figure 13. Fluctuation pressure $p'/(0.5\rho U_0^2)$ for phase- and spanwise-averaged flow fields, where T is the period at U_0 = 44 m/s, N = 5, and s/b = 6.0.

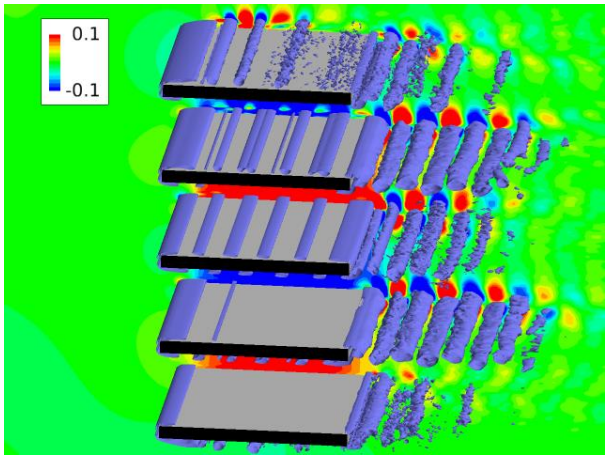

Figure 14. Iso-surfaces of the second invariant $(Q/(U_0/b)^2$ = 0.02) and fluctuation pressure $p'/(0.5\rho U_0^2)$ for phase-averaged flow fields at U_0 = 44 m/s, N = 5, and s/b = 6.0.

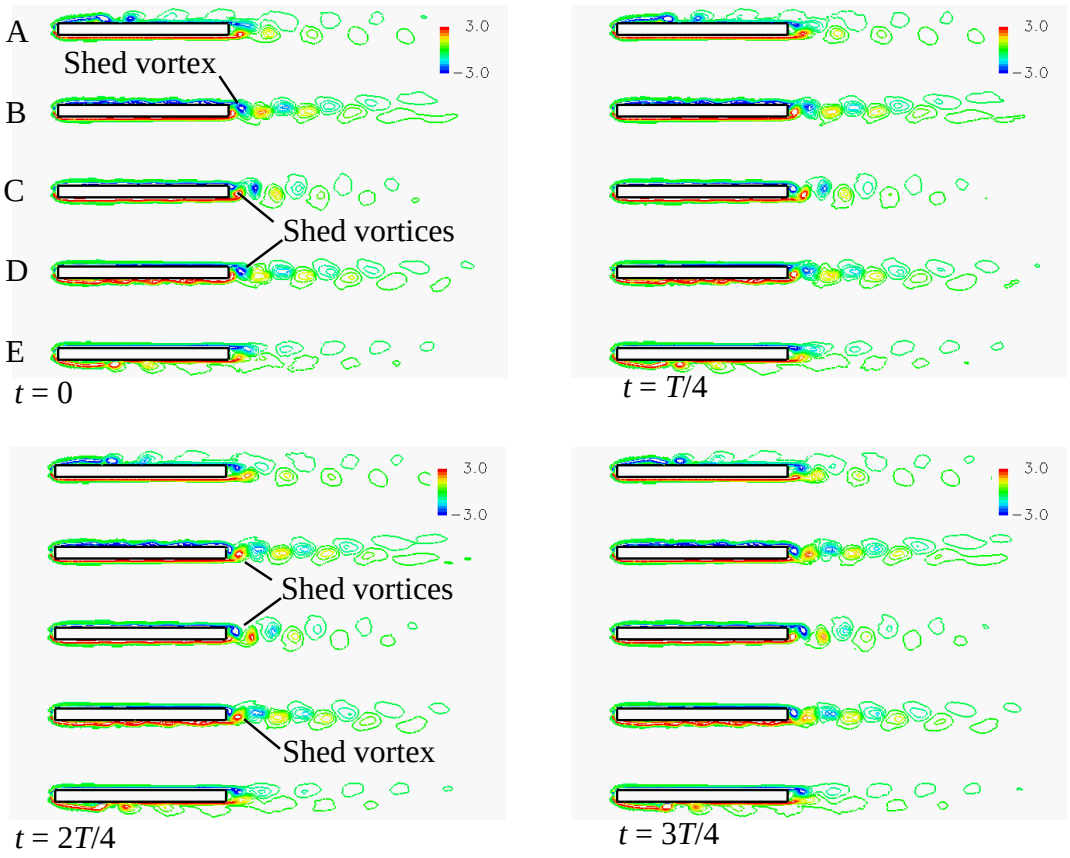

Figure 15. Vorticity $\omega_z/(U_0/b)$ (left) for phase- and spanwise-averaged flow fields for the resonant condition, where T is the period at U_0 = 44 m/s, N = 5, and s/b = 6.0.

D. Vortex shedding for small distance s/b

Figure 16 shows the RMS values of streamwise velocity fluctuations along x/b = 2.5. It is shown that the velocity fluctuations have sharp peaks in each wake of the plates for s/b = 3.0, 6.0 whereas those are overall intense for smaller distance.

Figure 17 shows the power spectra of the streamwise velocity fluctuations at the normal position for the most intense velocity fluctuations between the wakes of plates B, C along x/b = 2.5 (y/b = 0.5 (s/b = 6.0), y/b = 0.6 (s/b = 3.0), y/b = 0.5 (s/b = 1.5), y/b = 1.5 (s/b = 1.0), y/b = 1.2 (s/b = 0.5)).

As shown in Fig. 17, the two peaks of St = 0.16, 0.23 are found for s/b = 1.5, whereas the single peak of St = 0.21-0.22 is dominant for s/b = 3.0 and 6.0. Figure 18 shows the power spectra of the normal velocity fluctuations in each wake of plates A-E (y/b = 5.5, 3.0, 0.5, -2.0, and -4.5) for s/b = 1.5. This figure shows the peak at the above-mentioned higher frequency of St = 0.23 is dominant in each wake of plates B and D, whereas that at the lower frequency of St = 0.16 is dominant in the wake of plate C. The peaks for the outer plates of A, E are weak. These resutls show that the peak at the frequency of St = 0.16 and that of St = 0.23 as shown in Fig. 17 are corresponding to the vortex shedding in the narrow wakes of plates B and D and that in the wide wake of plate C, respectively. This variation of the frequency of the dominant vortex shedding in the wake of the plates inhibit the above-mentioned the synchronization of vortex shedding from the neighboring plates as discussed in Sec. V. C. This is the reason why the resonant acoustic radiation becomes weak for s/b = 1.5 in comparison with that for s/b = 3.0, 6.0.

As shown in Fig. 17, there is a intense peak at St = 0.27 for s/b = 1.0. This peak is due to the vortex shedding from the narrow wakes of plates B and D, whereas the vortex shedding from the wide wake of plate C is negligibly weak.

For s/b = 0.5, no intense peak is observed, although the small peak is observed at the fundamental frequency of St = 0.04. This indicates that intense vortex formation does not occur in the wake of each plate. Figure 19 shows the

contours of the fluctuation pressure for s/b = 0.5. As shown in this figure, large-scale low-pressure regions are formed in the wakes of the plate, and single bluff-body alternate vortex formation behaviour is observed. However, this formation is intermittent and not intense in comparison with the vortex shedding from each wake of the plates for the resonant condition for s/b = 3.0 and 6.0 as shown in Fig. 17.

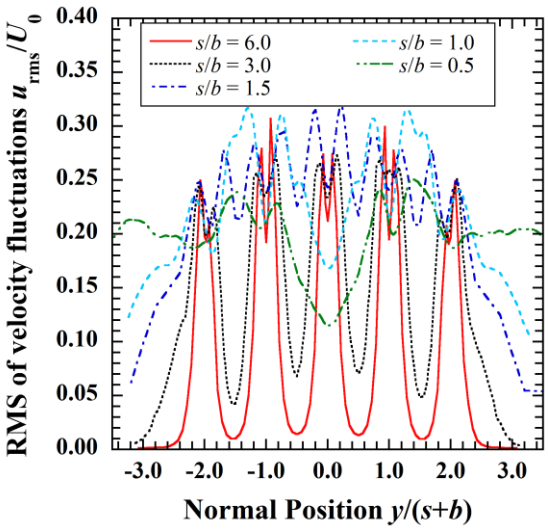

Figure 16. RMS values of velocity fluctuations u_{rms}/U_0 along x/b = 2.5.

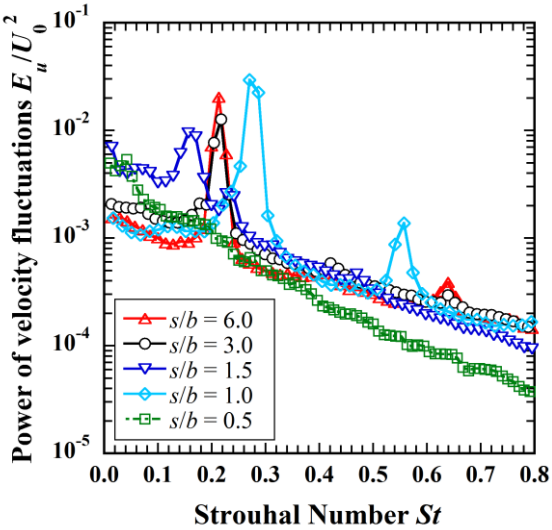

Figure 17. Power spectra of streamwise velocity fluctuations in the wake of plate C (y/b = 0.5 (s/b = 6.0), y/b = 0.6 (s/b = 3.0), y/b = 0.5 (s/b = 1.5), y/b = 1.5 (s/b = 1.0), y/b = 1.2 (s/b = 0.5)).

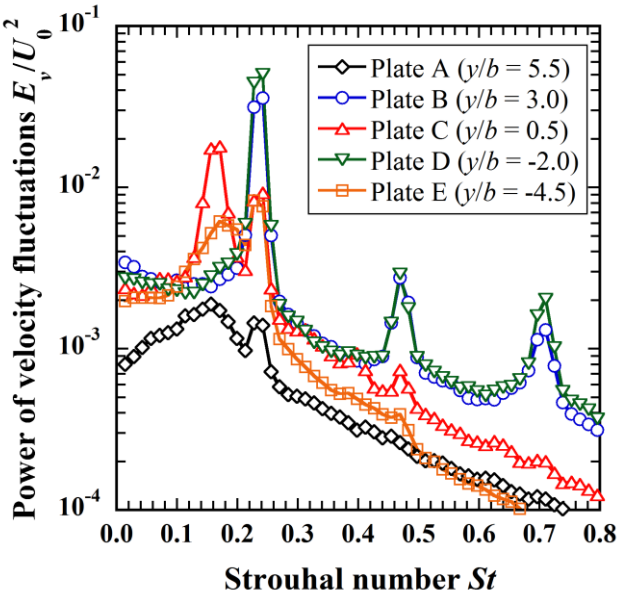

Figure 18. Power spectra of normal velocity fluctuations in the wakes of plates A-E (y/b = 5.5, y/b = 3.0, y/b = 0.5, y/b = -2.0, y/b = -4.5).

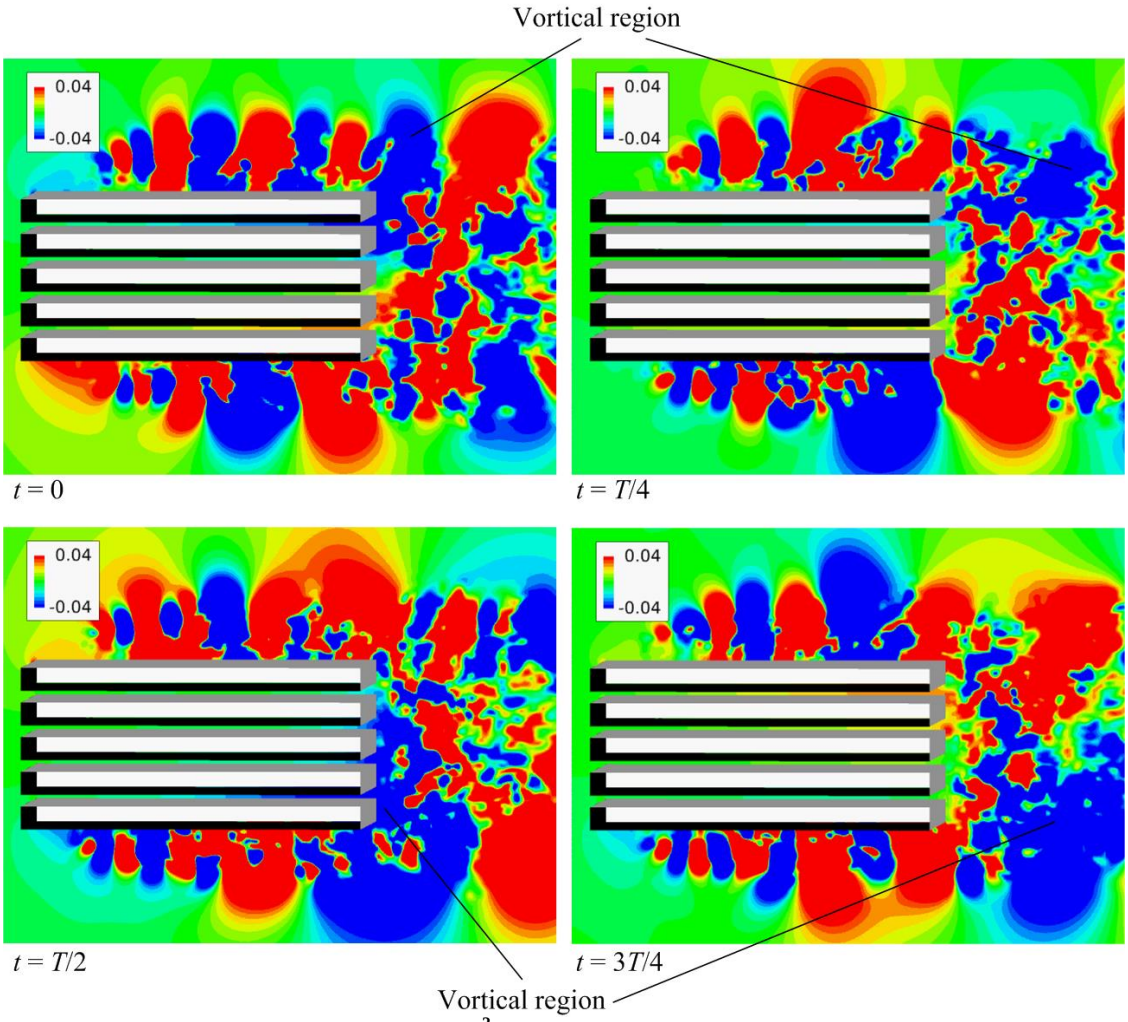

Figure 19. Fluctuation pressure $p'/(0.5\rho U_0^2)$, where T is the fundamental period (s/b = 0.5).

VI. Conclusion

Acoustic and flow fields around a cascade of flat plates were clarified by direct simulation of flow and acoustic fields and wind tunnel experiments. As a result, the ratio of the distance to the plate thickness, s/b, was found to affect both the fields significantly. For s/b = 3.0 and 6.0, the intense sound is radiating at specific velocity. At this time, the acoustic resonance occurs and the synchronization of vortex shedding from the neighboring plates occurs. For a larger distance of s/b = 13.0, the flow and acoustic fields around each plate approach those around a single plate, and the intense resonant acoustic radiation does not occur. For the small distance of s/b = 0.5-1.5, the biased flow pattern appears and the wake width varies for the neighbroing plates. For s/b = 1.0, 1.5, this variation causes the difference of the frequency of the vortex shedding from each plate and the above-mentioned synchronization is inhibited. As a result, the resonant acoustic radiation becomes weaker. For s/b = 0.5, the intense vortex formation does not occur in the wake of each plate, althogh single bluff-body alternate vortex formation behaviour is observed in the overall wakes of the plates.

Acknowledgments

The present study was supported by JSPS KAKENHI Grant of No. 24760134, that of No. 26820044 and through the Next-generation Supercomputer Strategy Program by the Ministry of Eduction, Culture, Sports, Science, and Technology of Japan (MEXT).

References

[1]Parker, R., "Resonance effects in wake shedding from parallel plates: Some experimental observations," *Journal of Sound and Vibration*, Vol. 4, 1966, pp. 62-72.

[2]Yokoyama, H., Kitamiya, K. and Iida, A., "Flows around a cascade of flat plates with acoustic resonance," *Physics of Fluids*, Vol. 25, 2013, 106104.

[3]Kumar, S. R., Sharma, A. and Agrawal, A., "Simulation of flow around a row of square cylinders," *Journal of Fluid Mechanics*, Vol. 606, 2008, pp. 369-397.

[4]Bearman, P. W. and Wadcock, A. J., "The interaction between a pair of circular cylinders normal to a stream," *Journal of Fluid Mechanics*, Vol. 61, 1973, pp. 499-511.

[5]Sumner, D., Wong, S. S. T., Price, S. J., Paidoussis, M. P., "Fluid Behaviour of Side-by-Side Circular Cylinders in Steady Cross-Flow," *Journal of Fluids and Structures*, Vol. 13, 1999, pp.309-338.

[6]Lele, S. K., "Compact finite difference schemes with spectral-like resolution," *Journal of Computational Physics*, Vol. 103, 1992, pp. 16-42.

[7]Rizzetta, D. P. and Visbal, M. R., "Large-Eddy Simulation of Supersonic Cavity Flow fields Including Flow Control," *AIAA Journal*, Vol. 41, 2003, pp. 1452-1462.

[8]Bogey, C. and Bailly, C., "Large eddy simulations of round free jets using explicit filtering with/without dynamic Smagorinsky model," *International Journal of Heat and Fluid Flow*, Vol. 27, 2006, pp. 603-610.

[9]Bogey, C. and Bailly, C., "Turbulence and energy budget in a self-preserving round jet: direct evaluation using large eddy simulation," *Journal of Fluid Mechanics*, Vol. 627, 2009, pp.129-160.

[10]Matsuura, K. and Kato, C., "Large-eddy simulation of compressible transitional flows in a low-pressure turbine cascade," *AIAA Journal*, Vol. 45, 2007, pp. 442-457.

[11]Gaitonde, D. V. and Visbal, M. R., "Pade-type higher-order boundary filters for the Navier-Stokes equations," *AIAA Journal*, Vol. 38, 2000, pp. 2103-2112.

[12]Thompson, K. W., "Time dependent boundary conditions for hyperbolic systems," *Journal of Computational Physics*, Vol. 68, 1987, pp. 1-24.

[13]Poinsot, T. J. and Lele, S. K., "Boundary conditions for direct simulations of compressible viscous flows," *Journal of Computational Physics*, Vol. 101, 1992, pp. 104-129.

[14]Kim, J. W. and Lee, D. J., "Generalized characteristic boundary conditions for computational aeroacoustics," *AIAA Journal* Vol. 38, 2000, pp. 2040-2049.